Supplementary information

A universal strategy for the hierarchical assembly of functional 0/2D nanohybrids

Yi-Tao Liu [a], Zhi-Qiang Duan [a], Xu-Ming Xie [a]* and Xiong-Ying Ye [b]

[a] Advanced Materials Laboratory, Department of Chemical Engineering, Tsinghua University,

Beijing 100084, China

[b] Department of Precision Instruments and Mechanology, Tsinghua University, Beijing 100084, China

* Corresponding author.

E-mail address: xxm-dce@mail.tsinghua.edu.cn

S1. Experimental details

S1.1 Raw materials

Natural graphite powder was purchased from Sinopharm Chemical Reagent Co., Ltd. Molybdenum disulfide (MoS_2) and hexagonal boron nitride (h-BN) powders were purchased from Sigma-Aldrich Co., LLC. Sodium dodecylbenzenesulfonate (SDBS) was purchased from Tianjin Jinke Fine Chemical Research Institute. Chloroauric acid ($HAuCl_4$) was purchased from Aladdin Industrial Inc. Sodium citrate dihydrate (SC) was purchased from Guangdong Chemical Reagent Engineering-Technological Research and Development Center. Ferric chloride anhydrous ($FeCl_3$) and ferrous chloride tetrahydrate ($FeCl_2 \cdot 4H_2O$) were purchased from Xilong Chemical Co., Ltd. Copper sulfate pentahydrate ($CuSO_4 \cdot 5H_2O$) and rhodamine 6G (Rh6G) were purchased from Sigma-Aldrich Co., LLC. Hydrochloric acid (HCl), sulfuric acid (H_2SO_4), 30% hydrogen peroxide (H_2O_2) and sodium hydroxide (NaOH) were purchased from Beijing Chemical Works.

S1.2 Exfoliation of 2D materials

The procedures for exfoliating natural graphite, MoS_2 and h-BN powders into 2D materials were adapted from the previous reports [1,2]. Briefly, the powders were added to 1 wt % SDBS aqueous solutions at an initial concentration of 5 mg mL^{-1}, and subjected to sonication at 300 W for 4 h. The obtained slurries were centrifuged at 4400 rpm for 45 min, and the top 1/2 supernatants were collected, yielding aqueous solutions of single- and few-layer 2D materials. SDBS served as a surfactant to stabilize the 2D materials in water, and endowed them with carboxylate groups for Cu(II) ion coordination.

S1.3 Synthesis of Au NPs

The synthesis of Au NPs followed a mature route [3]. Briefly, 0.01 wt % $HAuCl_4$ aqueous solution 50 mL

was heated to boiling, to which 1 wt % SC aqueous solution 0.5 mL was added. In ~2 min, the mixed solution turned to light blue and then to brilliant red, indicating the formation of Au NPs. The boiling state was kept for 20 min to complete the reduction process. The obtained Au NPs were monodisperse, and had a regular spherical morphology. SC served as a reducer and a surfactant to stabilize the Au NPs in water, and endowed them with carboxylate groups for Cu(II) ion coordination.

S1.4 Synthesis of Fe_3O_4 NPs

The synthesis of Fe_3O_4 NPs was reported elsewhere [4]. Briefly, 12.1 N HCl 0.85 mL and purified deoxygenated water 25 mL were mixed, in which $FeCl_3$ 5.2 g and $FeCl_2 \cdot 4H_2O$ 3.14 g were successively dissolved under stirring. The resulting solution was dropped in 1.5 M NaOH 250 mL under vigorous stirring, generating an instant black precipitate. The precipitate was attracted by a strong magnet, collected, and dispersed in purified deoxygenated water 250 mL under stirring. The above procedures were repeated 3-5 times until the pH was ~8. The obtained Fe_3O_4 NPs were finally dissolved in 1 wt % SDBS aqueous solution under stirring. SDBS served as a surfactant to stabilize the Fe_3O_4 NPs in water, and endowed them with carboxylate groups for Cu(II) ion coordination. Note that to prepare monodisperse Fe_3O_4 NPs, it was important to carry out the above reaction in an aqueous solution with an Fe(II)/Fe(III) mol ratio of 0.5 and a pH of 11-12.

S1.5 Hierarchical assembly of functional 0/2D nanohybrids

In a typical run, the aqueous solutions of NPs and 2D materials were mixed at different ratios, to which a small volume of $CuSO_4$ aqueous solution was added. It should be stressed that too many Cu(II) ions would cause serious aggregation or even precipitation. The mixed solution was kept for 48 h to allow complete assembly. Note that during the assembly process the mixed solution was subjected to gentle sonication (50 W) to prevent precipitation. Thereafter, the mixed solution was centrifuged at 8000 rpm for 30 min. The

precipitate was collected, and re-dispersed in water under sonication at a concentration of 0.1 mg mL^{-1}.

S1.6 Preparation of SERS samples

For SERS testing, bare SiO$_2$/Si wafers (~10 × 10 mm^2) were firstly soaked in Piranha solution (a mixture of H$_2$SO$_4$ and 30% H$_2$O$_2$ at a vol ratio of 7 : 3) at 60 ^{o}C for 30 min. The aqueous solutions of Au NPs and 0/2D nanohybrids 50 μL were dropped on SiO$_2$/Si wafers and blow-dried by nitrogen, respectively. Then 2 μM Rh6G aqueous solution 50 μL was dropped on bare, Au-coated and 0/2D nanohybrid-coated SiO$_2$/Si wafers and blow-dried by nitrogen, respectively.

S1.7 Equipment

TEM was performed by a Hitachi H7700 operated at an accelerating voltage of 100 kV. HRTEM was performed by a JEOL JEM-2010 operated at an accelerating voltage of 120 kV. AFM was performed by a Shimadzu SPM-9500 in the tapping mode. Raman spectra were recorded by a Horiba LabRam H-800 spectrometer with 633 nm laser excitation. UV-vis spectra were recorded by a Pgeneral TU-1810 twin-beam spectrophotometer from 200 to 900 nm.
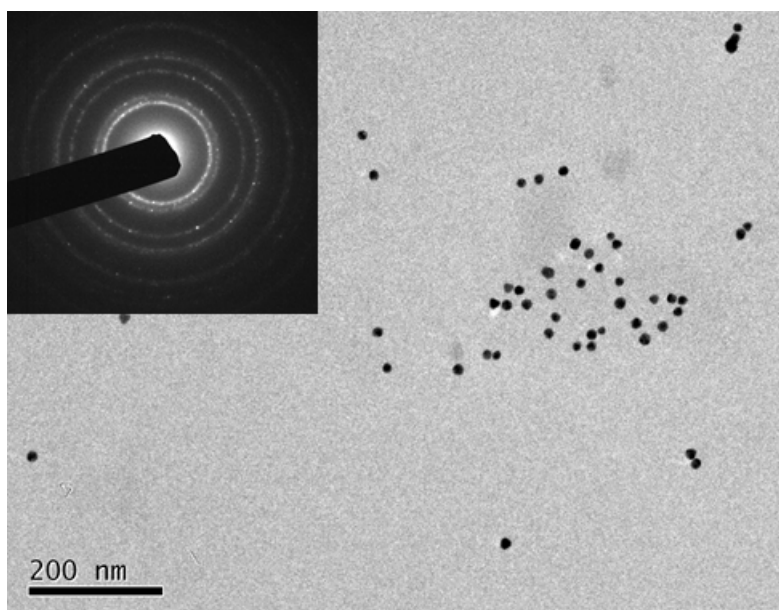
S2. TEM and AFM images of Au NPs

Fig. S1. TEM image of as-synthesized Au NPs and the corresponding ED pattern.
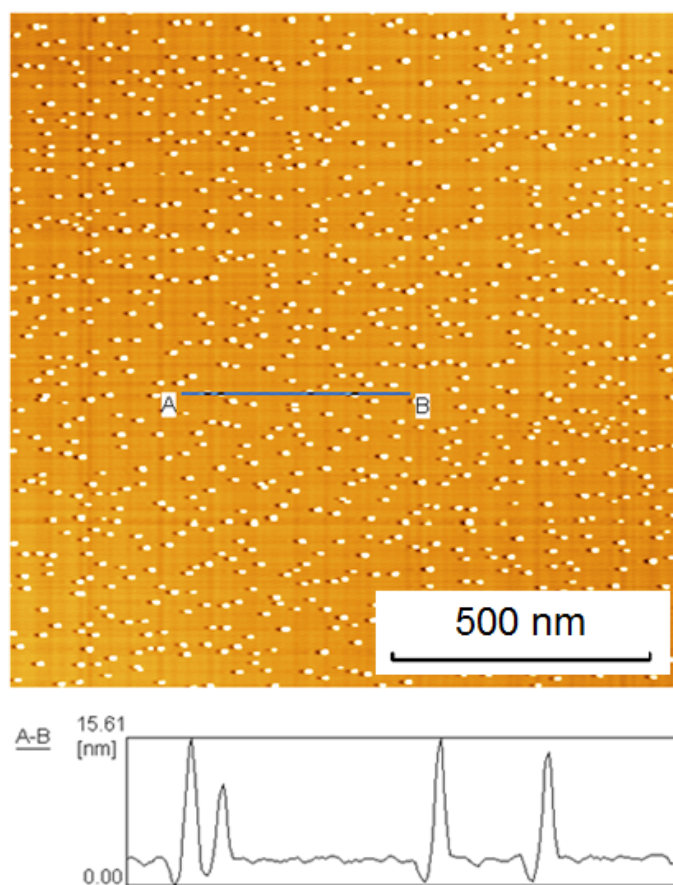

Fig. S2. AFM image of as-synthesized Au NPs and the height profile corresponding to the blue line.
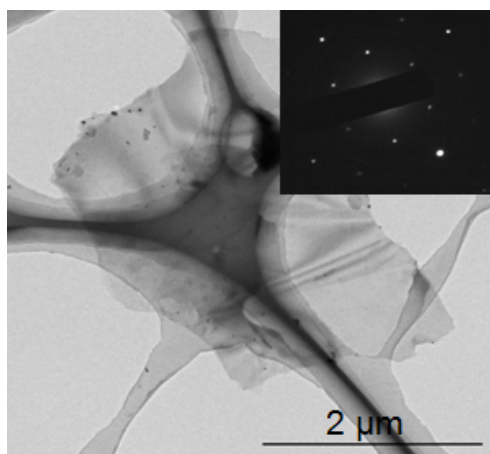
S3. TEM images of 2D materials

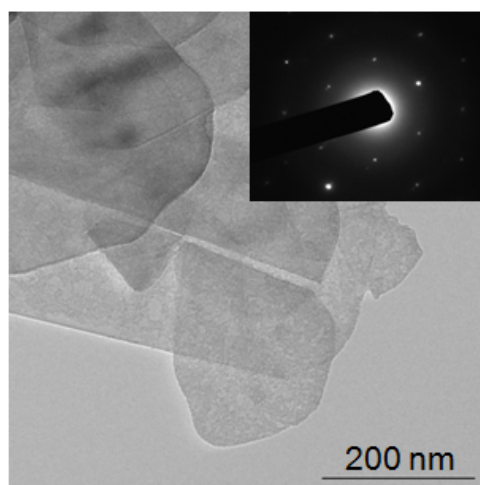**Fig. S3.** TEM image of a pristine graphene nanosheet and the corresponding ED pattern.

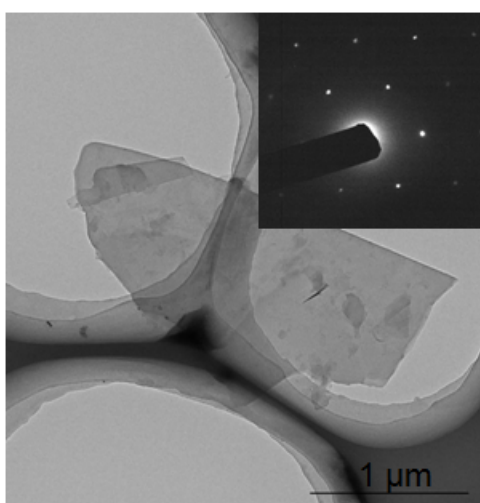**Fig. S4.** TEM image of a h-BN nanosheet and the corresponding ED pattern.

Fig. S5. TEM image of a MoS_2 nanosheet and the corresponding ED pattern.
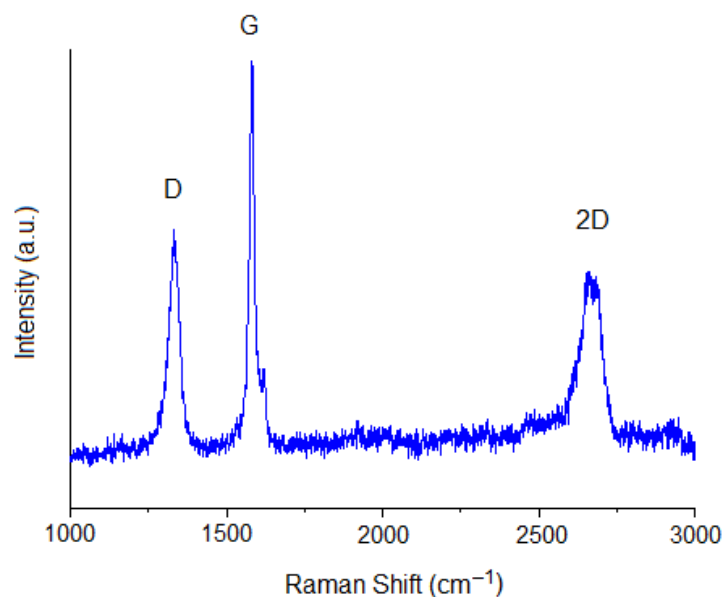
S4. *Raman spectra of 2D materials*

Fig. S6. Raman spectrum of pristine graphene nanosheets, showing a D peak at ~1350 cm^{-1}, a G peak at ~1580 cm^{-1} and a 2D peak at ~2700 cm^{-1}. The D peak is defect-related, and arises from the activation in the first order scattering of the sp^3-bonded carbon atoms in the graphitic sheets. The G peak corresponds to the E$_{2g}$ mode, and is related to the vibration of the sp^2-bonded carbon atoms in the graphitic sheets. The 2D peak is the second order of the D peak [5].
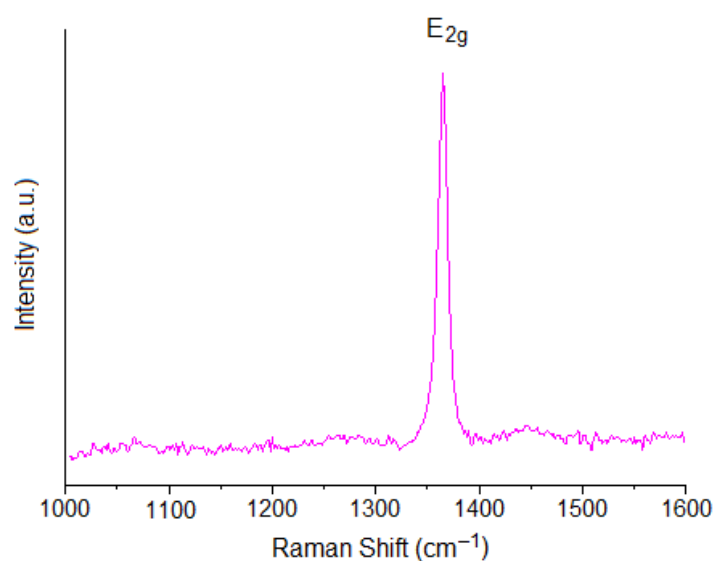

Fig. S7. Raman spectrum of *h*-BN nanosheets, showing a characteristic peak at ~1365 cm^{-1} attributed to the B–N high-frequency vibrational mode (E$_{2g}$) within the BN layers [6].
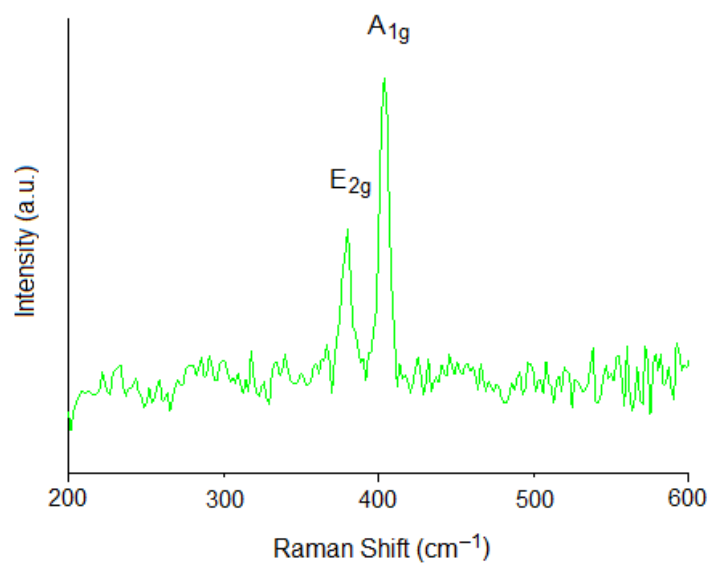
Fig. S8. Raman spectrum of MoS_2 nanosheets, showing characteristic peaks at ~381 and 407 cm^{-1} corresponding to the in-plane E_{2g} and out-of plane A_{1g} vibrations, respectively [7].

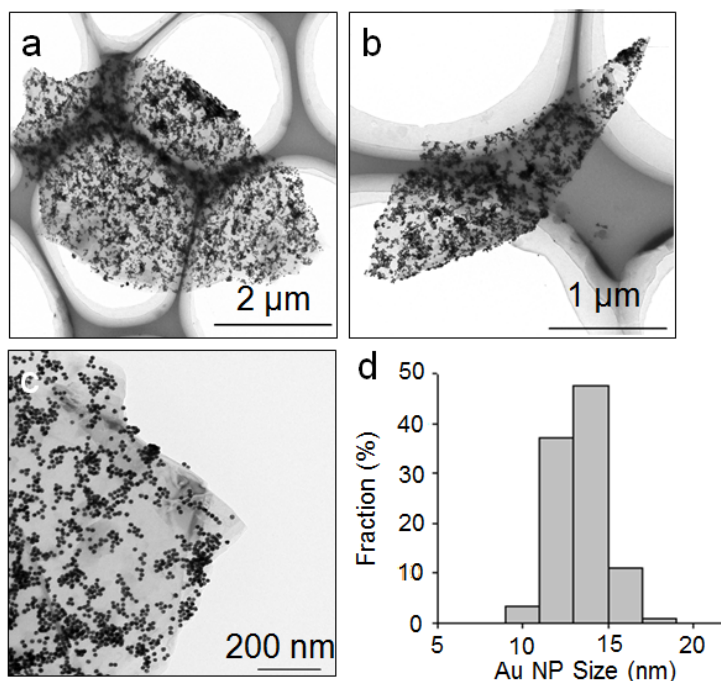## *S5. TEM and AFM images of Cu(II)-coordinated G/Au nanohybrid*

Fig. S9. (a), (b) Low and (c) high-magnification TEM images of a Cu(II)-coordinated G/Au nanohybrid (G/Au wt ratio = 20); (d) statistics on the Au NP size distribution based on TEM images, indicating that the Au NPs are monodisperse with more than 80% having particle sizes within 11-15 nm.

It should be stressed that our strategy yields a narrower size distribution than the solution-phase *in situ* growth of NPs. For example, Guardia et al. reported the synthesis of Au NPs decorated on *r*-GO by the simultaneous reduction of a mixed solution of $HAuCl_4$ and GO by UV irradiation without or with citric acid [8]. Statistics showed that there were ~60% Au NPs within 13-17 nm (average = 14.6 nm) in the absence of citric acid, and ~40% Au NPs within 18-22 nm (average = 19.7 nm) in the presence of citric acid. Besides, since Au^{3+} ions were selectively adsorbed to the defects (oxygen-containing groups) of GO through electrostatic attraction, Au NPs thus grown were only sparsely and ununiformly attached to the GO surface. Another case was Ag NPs decorated on *h*-BN [9]. It was reported that Ag NPs could be grown on the *h*-BN surface *in situ* in aqueous solution. However, due to the higher chemical inertness of *h*-BN than GO, Ag NPs thus grown were highly irregular in both shape and size, ranging from 20 nm to 80 nm.

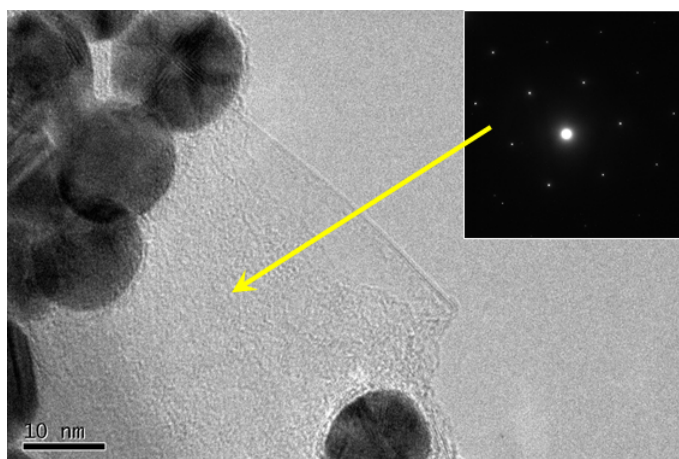## S6. HRTEM images of Cu(II)-coordinated 0/2D nanohybrids

Fig. S10. HRTEM image of a Cu(II)-coordinated G/Au nanohybrid and the corresponding ED pattern.
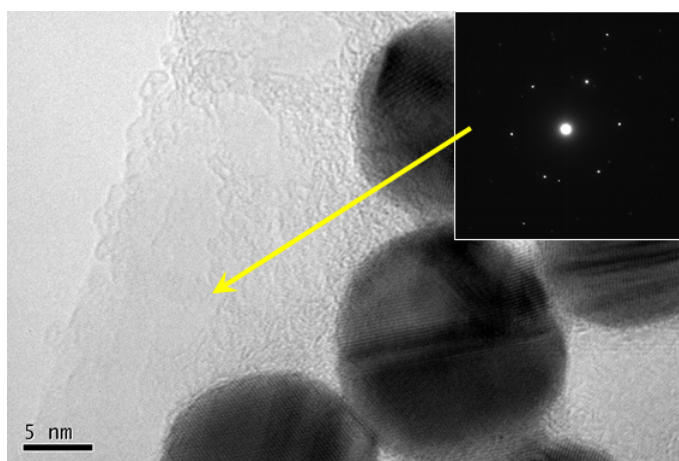

Fig. S11. HRTEM image of a Cu(II)-coordinated h-BN/Au nanohybrid and the corresponding ED pattern.

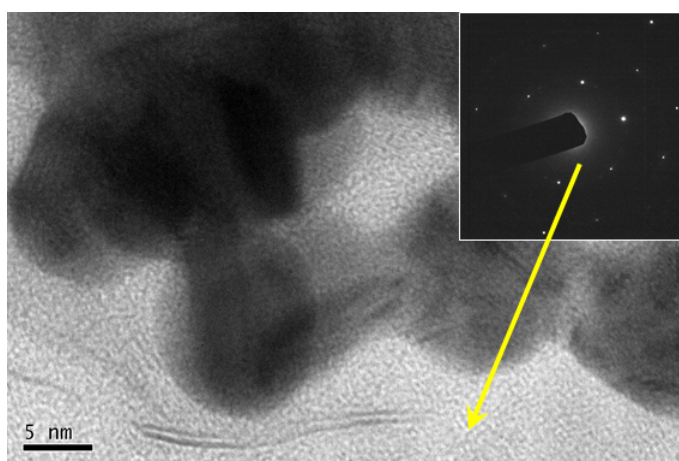**Fig. S12.** HRTEM image of a Cu(II)-coordinated MoS_2/Au nanohybrid and the corresponding ED pattern.

S7. Atomically resolved HRTEM image of Cu(II)-coordinated MoS$_2$/Au nanohybrid

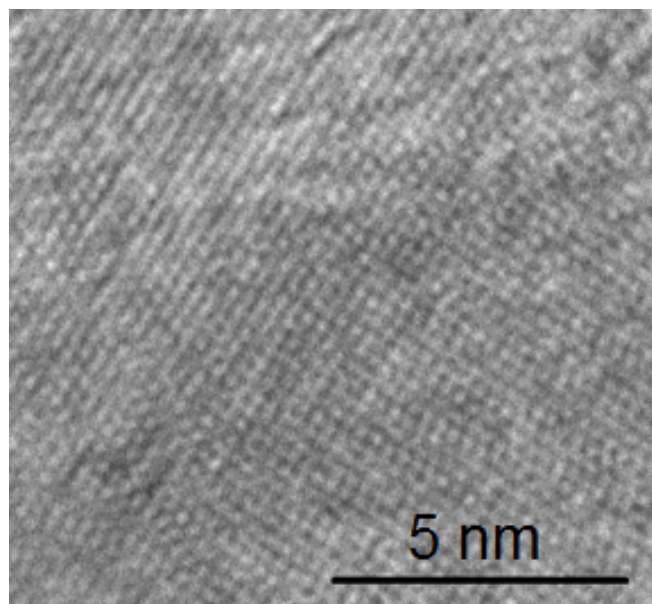**Fig. S13.** Atomically resolved HRTEM image of a Cu(II)-coordinated MoS$_2$/Au nanohybrid, indicating this coordination strategy is noninvasive since the hexagonal symmetry of MoS$_2$ is largely preserved.

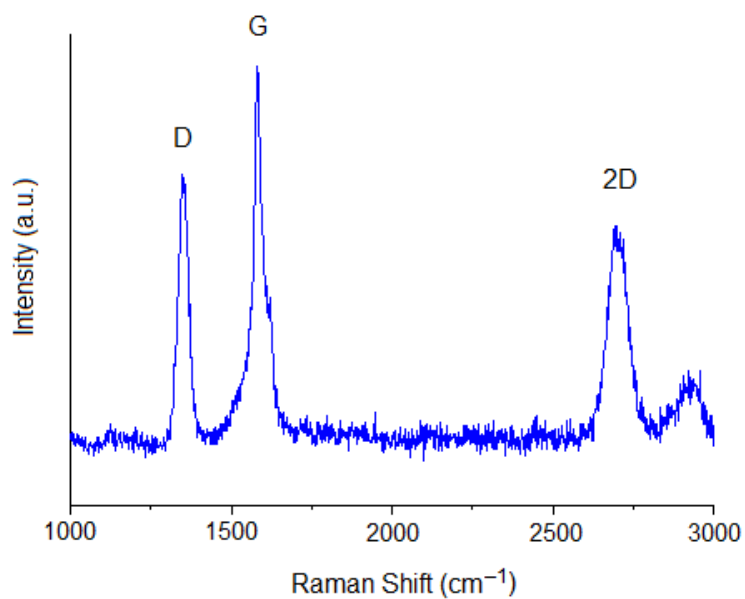## S8. HRTEM images of Cu(II)-coordinated 0/2D nanohybrids

Fig. S14. Raman spectrum of a Cu(II)-coordinated G/Au nanohybrid.
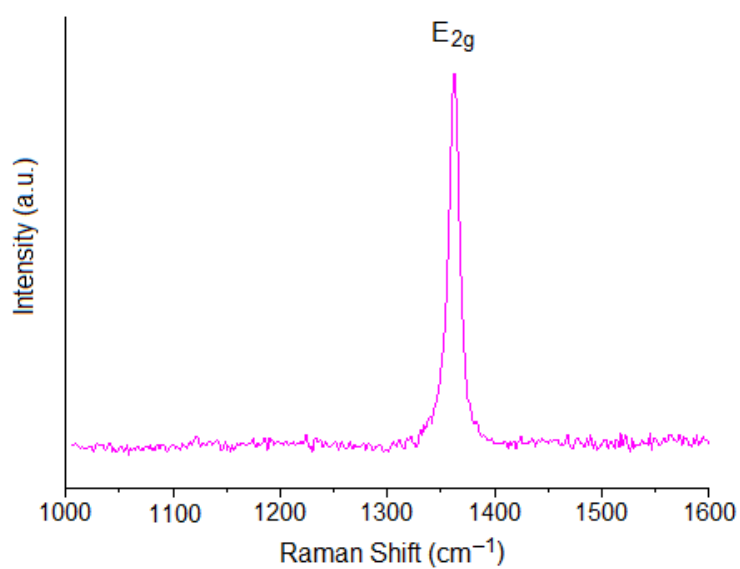
Fig. S15. Raman spectrum of a Cu(II)-coordinated *h*-BN/Au nanohybrid.
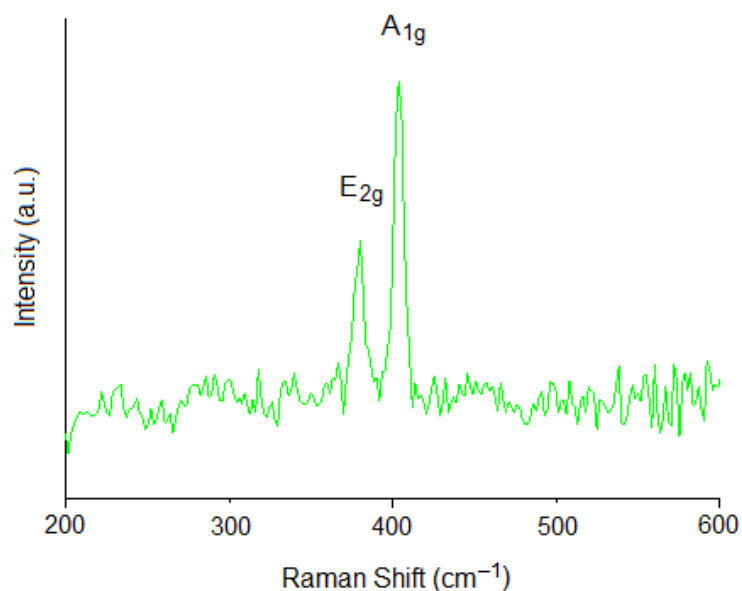
Fig. S16. Raman spectrum of a Cu(II)-coordinated MoS_2/Au nanohybrid.

After being coordinated with Au NPs, these 2D materials do not have any significant changes in their Raman spectra in terms of peak shape and position. The similar Raman patterns before and after coordination indicate that the overall lattice structure of these 2D materials is preserved, and there are few, if any, defects induced by coordination. The Raman results are consistent with the above atomically resolved HRTEM observation (Fig. S13), and are also consistent with the previous reports on the GO coordination by ourselves and others [10-12].

S9. UV-vis spectra of Cu(II)-coordinated h-BN/Au nanohybrid

Fig. S17. UV-vis spectra of the aqueous solutions of Au NPs (yellow), *h*-BN (purple) and *h*-BN/Au NPs before (blue) and after (red) Cu(II) ion coordination. It is found for Au NPs t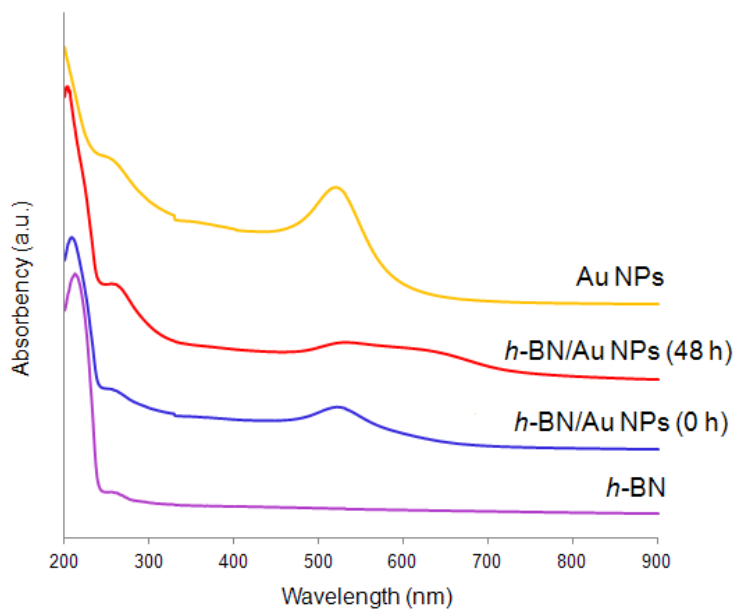hat a rather broad absorption band shifting to higher wavelength is verified after 48 h, corresponding to the NP aggregation due to coordination [13,14]. This is also the case for the graphene and MoS$_2$/Au NPs systems.

S10. SERS spectra of Cu(II)-coordinated G/Au nanohybrids with different loading densities
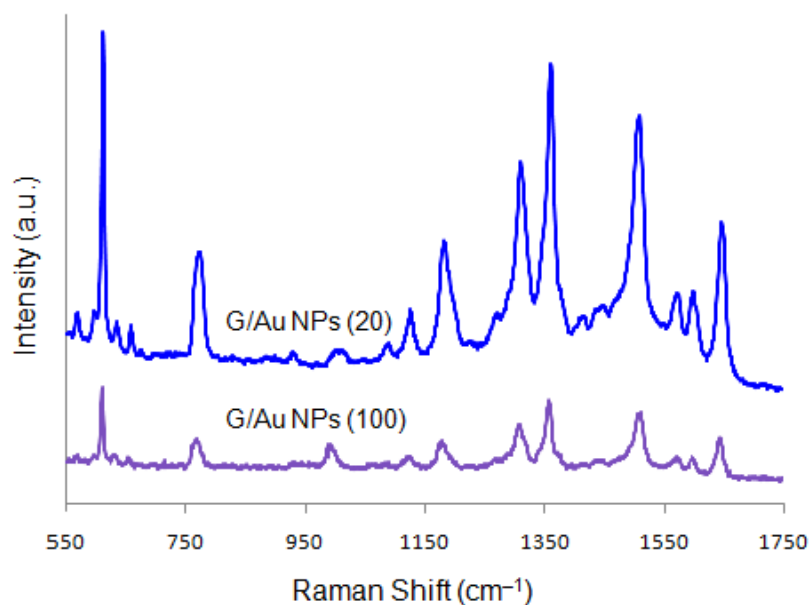

Fig. S18. SERS spectra of Cu(II)-coordinated G/Au nanohybrids at wt ratios of 100 and 20, respectively.

We try to discuss the SERS effects of the Cu(II)-coordinated 0/2D nanohybrids here. Although SERS has been discovered for more than three decades [15], its mechanisms remain an active research topic. Generally, two major factors are agreed on the relative significance of the proposed mechanisms, i.e., chemical enhancement and electromagnetic enhancement. In the chemical enhancement mechanism, a charge-transfer state is created between the metal NPs and the adsorbate molecules. In a manner analogous to that observed in resonance Raman spectroscopy, the existence of this charge-transfer state increases the probability of a Raman transition by providing a pathway for resonant excitation. This mechanism is site-specific and analyte-dependent. In the electromagnetic enhancement mechanism, one must consider the size, shape and material of the nanoscale roughness features. Although the two mechanisms are often thought to be independent, it has recently been suggested that they are intimately linked [16], but one or the other may dominate at a given excitation wavelength.

When Au NPs are dropped on a SiO$_2$/Si wafer directly from the colloid, they are uniformly and sparsely distributed on the wafer, as shown in Fig. S2. These isolated Au NPs result in fewer "hot spots" and thus a weaker SERS signal. After the hierarchical assembly, however, Au NPs are densely packed on the surface of the 2D materials, which translates into a high loading density. The high loading density of Au NPs is advantageous for the enrichment of the Rh6G molecules in the process of SERS detection, and more "hot spots" are formed in the nanoscale junctions and interstices. Therefore, the dipoles induced by the plasmon resonance will couple and transmit on the whole substrates. Besides, the electrostatic attraction between the positively charged Rh6G molecules and the negatively charged 2D materials (due to the presence of SDBS) can further increase the concentration of Rh6G in the vicinity of Au NPs. The large specific surface areas of the underlying 2D materials facilitate better enrichment of the Rh6G molecules, thus significantly enhancing the SERS signal of Rh6G as compared with that of Au NPs in the colloid.

Moreover, it is reported that the work functions of Au, graphene, MoS$_2$ and *h*-BN are 5.1 eV, 4.42 eV, 4.6−4.9 eV and 4.26 eV, respectively [17-20]. Since the work functions of these 2D materials are very close to that of Au, we can expect easy charge transfer from them to Au, as was suggested between carbon nanotubes and Au [21]. It is not very clear why graphene has a better SERS effect than MoS$_2$ and *h*-BN at the present stage. We infer that it may be attributed to the better charge-transfer effect between graphene and Au. Also we note that the average size of the graphene nanosheets obtained in our experiment is much larger than that of MoS$_2$ or *h*-BN, thus resulting in a higher loading density of Au NPs.

We further compare the SERS spectra of the Cu(II)-coordinated G/Au nanohybrids at G/Au wt ratios of 100 and 20, as shown in Fig. S18. It is worth noting that the two SERS spectra do not have any significant changes in terms of profile. However, the Raman intensity increases sharply with the increase of the Au fraction. This phenomenon can be attributed to the increasing loading density of Au NPs on the surface of graphene as the "hot spots" for strong localized electromagnetic fields produced by the gaps between neighboring Au NPs. Further work is being done in our laboratory to elucidate this phenomenon.

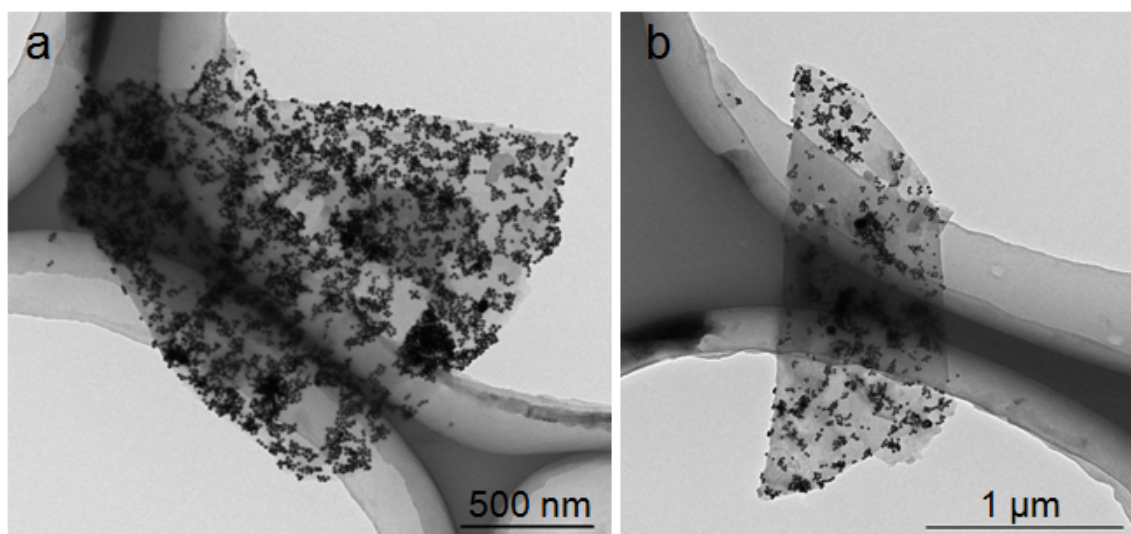## S11. TEM images of Fe(III)- and Ag(I)-coordinated h-BN/Au nanohybrids

Fig. S19. TEM images of (a) Fe(III)- and (b) Ag(I)-coordinated G/Au nanohybrids.

Other than divalent metal ions such as Cu(II), trivalent and monovalent metal ions have also been used to form 0/2D nanohybrids through coordination. For example, Fe (III) and Ag(I) have been tested because both have coordination abilities to carbonyls [22,23]. It is worth noting, however, that the coordination stability constant of Fe (III) is much higher than that of Ag(I), and the latter even fails to coordinate to the oxygen moieties on GO [24]. Fig. S19 shows the 0/2D nanohybrids of pristine graphene and Au NPs through coordination with Fe(III) and Ag(I), respectively. It is found, interestingly, that in both cases coordinated G/Au nanohybrids are successfully formed. It is understandable since even Ag(I) can effectively coordinate to SDBS and SC [25-27]. The difference in the coordination stability constants of Fe (III) and Ag(I), however, contributes to their different coordination performances. In Fig. S19a, Au NPs are easily and densely attached to the graphene surface, emphasizing the stronger coordination ability of Fe (III) to carbonyls. In Fig. S19b, Au NPs are only sparsely and ununiformly distributed on the graphene surface, probably due to the weaker coordination ability of Ag(I) to carbonyls, which translates to a lower reaction rate.

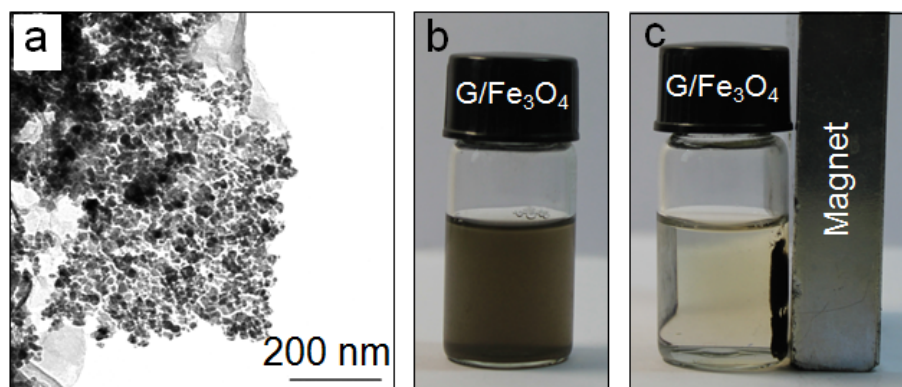### *S12. TEM and digital images of Cu(II)-coordinated G/Fe$_3$O$_4$ nanohybrid*

Fig. S20. TEM image of a Cu(II)-coordinated G/Fe$_3$O$_4$ nanohybrid (G/Fe$_3$O$_4$ wt ratio = 5); (b) and (c) digital images of its aqueous solution before and after magnetic attraction.

To test the versatility of this coordination strategy on other NPs, we have assembled magnetic Fe$_3$O$_4$ NPs on pristine graphene, as shown in Fig. S20. The obtained Cu(II)-coordinated G/Fe$_3$O$_4$ nanohybrid can be dispersed in water, forming a dark-colored magnetic fluid that is easily recyclable by a magnet. The G/Fe$_3$O$_4$ nanohybrid has substantial potentials in catalysis, dye adsorption, magnetic resonance imaging and drug delivery [28-30].

S13. Supplementary References

[1] L. Guardia, M. J. Fernández-Merino, J. I. Paredes, P. Solís-Fernández, S. Villar-Rodil, A. Martínez-Alonso and J. M. D. Tascón, *Carbon*, 2011, **49**, 1653.

[2] R. J. Smith, P. J. King, M. Lotya, C. Wirtz, U. Khan, S. De, A. O'Neill, G. S. Duesberg, J. C. Grunlan, G. Moriarty, J. Chen, J. Wang, A. I. Minett, V. Nicolosi and J. N. Coleman, *Adv. Mater.*, 2011, **23**, 3944.

[3] G. Frens, *Nature Phys. Sci.*, 1973, **241**, 20.

[4] Y. S. Kang, S. Risbud, J. F. Rabolt and P. Stroeve, *Chem. Mater.*, 1996, **8**, 2209.

[5] M. S. Dresselhaus, A. Jorio, M. Hofmann, G. Dresselhaus and R. Saito, *Nano Lett.*, 2010, **10**, 751.

[6] A. Pakdel, C. Zhi, Y. Bando, T. Nakayama and D. Golberg, *ACS Nano*, 2011, **5**, 6507.

[7] C. Lee, H. Yan, L. E. Brus, T. F. Heinz, J. Hone and S. Ryu, *ACS Nano*, 2010, **4**, 2695.

[8] L. Guardia, S. Villar-Rodil, J. I. Paredes, R. Rozada, A. Martínez-Alonso and J. M. D. Tascón, *Carbon*, 2012, **50**, 1014.

[9] Y. Lin, C. E. Bunker, K. A. Shiral Fernando and J. W. Connell, *ACS Appl. Mater. Interfaces*, 2012, **4**, 1110.

[10] S. Park, K.-S. Lee, G. Bozoklu, W. Cai, S. T. Nguyen and R. S. Ruoff, *ACS Nano*, 2008, **2**, 572.

[11] Y.-T. Liu, Q.-P. Feng, X.-M. Xie and X.-Y. Ye, *Carbon*, 2011, **49**, 3371.

[12] Y.-T. Liu, M. Dang, X.-M. Xie, Z.-F. Wang and X.-Y. Ye, *J. Mater. Chem.*, 2011, **21**, 18723.

[13] G. Goncalves, P. A. A. P. Marques, C. M. Granadeiro, H. I. S. Nogueira, M. K. Singh and J. Grácio, *Chem. Mater.*, 2009, **21**, 4796.

[14] T. J. Norman Jr., C. D. Grant, D. Magana, J. Z. Zhang, J. Liu, D. Cao, F. Bridges, A. van Buuren, *J. Phys. Chem. B*, 2002, **106**, 7005.

[15] D. L. Jeanmaire and R. P. J. Van Duyne, *Electroanal. Chem.*, 1977, **84**, 1.

[16] J. R. Lombardi and R. L. Birke, *J. Phys. Chem. C*, 2008, **112**, 5605.

[17] D. Dulić, S. J. van der Molen, T. Kudernac, H. T. Jonkman, J. J. D. de Jong, T. N. Bowden, J. van Esch,

B. L. Feringa and B. J. van Wees, *Phys. Rev. Lett.*, 2003, **91**, 207402.

[18] R. Czerw, B. Foley, D. Tekleab, A. Rubio, P. M. Ajayan and D. L. Carroll, *Phys. ReV. B*, 2002, **66**, 033408.

[19] K.-K. Liu, W. Zhang, Y.-H. Lee, Y.-C. Lin, M.-T. Chang, C.-Y. Su, C.-S. Chang, H. Li, Y. Shi, H. Zhang, C.-S. Lai and L.-J. Li, *Nano Lett.*, 2012, **12**, 1538.

[20] M. Morscher, M. Corso, T. Greber and J. Osterwalder, *Surf. Sci.*, 2006, **600**, 3280.

[21] J. W. G. Wildöer, L. C. Venema, A. G. Rinzler, R. E. Smalley and C. Dekker, *Nature*, 1998, **391**, 59.

[22] J.-J. Brunet, R. Chauvin, O. Diallo, F. Kindela, P. Leglaye and D. Neibecker, *Coord. Chem. Rev.*, 1998, **178–180**, 331.

[23] A. Grodzicki, I. Łakomska, P. Piszczek, I. Szymańska and E. Szłyk, *Coord. Chem. Rev.*, 2005, **249**, 2232.

[24] H. Bai, C. Li, X. Wang and G. Shi, *J. Phys. Chem. C*, 2011, **115**, 5545.

[25] Y. Song, J. Zhou, X. Lan, J. Zhou and Y. Yang, *Adv. Mater. Res.*, 2011, **233-235**, 1911.

[26] L. Hua, J. Chen, L. Ge and S. N. Tan, *J. Nanopart. Res.*, 2007, **9**, 1133.

[27] F.-K. Liu, P.-W. Huang, Y.-C. Chang, F.-H. Ko and T.-C. Chu, *J. Mater. Res.*, 2004, **19**, 469.

[28] S. Wu, Q. He, C. Zhou, X. Qi, X. Huang, Z. Yin, Y. Yang and H. Zhang, *Nanoscale*, 2012, **4**, 2478.

[29] Z. Geng, Y. Lin, X. Yu, Q. Shen, L. Ma, Z. Li, N. Pan and X. Wang, *J. Mater. Chem.*, 2012, **22**, 3527.

[30] X. Yang, X. Zhang, Y. Ma, Y. Huang, Y. Wang and Y. Chen, *J. Mater. Chem.*, 2009, **19**, 2710.